Communication

Molecular Synchronization Enhances Molecular Interactions: An Explanatory Note of Pressure Effects

Munenori Numata * and Chisako Kanzaki

Department of Biomolecular Chemistry, Graduate School of Life and Environmental Sciences, Kyoto Prefectural University, Shimogamo, Sakyo-ku, Kyoto 606-8522, Japan; s818631012@kpu.ac.jp

* Correspondence: numata@kpu.ac.jp; Tel.: +81-75-703-5132

check for updates

Abstract: In this study, we investigated a unique aspect of the supramolecular polymerization of tetrakis (4-sulfonatophenyl) porphyrin (TPPS), a self-assembling porphyrin, under non-equilibrium conditions by subtracting the effects of back-pressure on its polymerization. We focused on the enhanced self-assembly abilities of TPPS under a process of rapid proton diffusion in a microflow channel. Rapid protonation caused synchronization of many sets of protonation/deprotonation equilibria on the molecular scale, leading to the production of many sets of growing suparmolecular spices. Pressure effects in the microflow channel, which could potentially promote self-assembly of TPPS, were negligible, becoming predominant only when the system was in the synchronized state.

Keywords: supramolecular chemistry; microflow; non-equilibrium

1. Introduction

Anomalous amplification of weak interactions through synchronized behavior of components is ubiquitous in Nature on many scales, from elementary particles to the global scale. In contrast, the synchronous behavior, which should seriously affect material properties, of molecules has not been paid much attention by the chemistry community. Earlier, we proposed the possibility that molecules could be synchronized under very rapid environmental changes (e.g., pH or solvent polarity) in flowing micro-solutions [1,2]. Although those results were very primitive, we established simple models for chemists to consider the synchronized behaviors of molecules.

We have employed tetrakis (4-sulfonatophenyl) porphyrin (TPPS, with H_2TPPS and H_4TPPS representing its free and protonated forms, respectively) as a model compound for such studies (Figure 1) [3–8]. J-aggregates formation is triggered by protonation of the central pyrrole groups. The driving force for self-assembly of the resultant H_4TPPS is hydrogen bonding and other electrostatic intermolecular interactions. In a bulk solution, TPPS self-assembles into J-aggregates under acidic conditions, where protonation/deprotonation processes between H_2TPPS and H_4TPPS are under equilibrium. The efficiency of J-aggregate formation is governed predominantly by the concentration of H_4TPPS; therefore, J-aggregate formation is accelerated at lower values of pH. In contrast to this general behavior in solution, we have found that the efficiency of J-aggregate formation is correlated to the time required for protonation of H_4TPPS [1]. Very rapid proton diffusion in a microflow channel [9–14] results in increasing temporal H_4TPPS concentrations, even at a constant value of pH [15,16].

In the present study, we have employed focusing hydrodynamic flow as self-assemble fields [17–19], where the central flow is the main channel along which self-assembly proceeds with time and aqueous HCl solutions are injected from the side flow (Figure 2). The time required for complete diffusion, the residence time in the channel, and final pH values are precisely regulated by changing the flow rate ratios, which enable precise control over the self-assembly dynamics.

Flowing TPPS molecules in a micro-channel are always under the influence of back-pressure. We have demonstrated recently that J-aggregate formation can also be accelerated by back-pressure in a micro-channel [2]. Accordingly, precise evaluation of the effect of simultaneous protonation of H_2TPPS on its self-assembly should carefully subtract the effect of back-pressure. In this present study, we found that pressure effects have little influence on the overall self-assembly behavior, strongly supporting our finding that very rapid protonation and adjusting time phases of protonation/deprotonation oscillation play essential roles leading to overall acceleration of the self-assembly process.
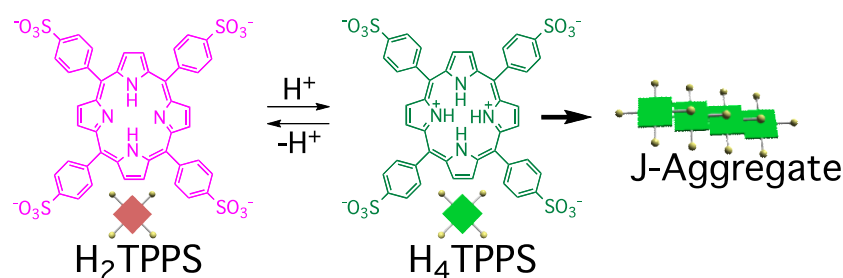

Figure 1. Molecular structure of TPPS and a schematic representation of its J-aggregate formation under acidic conditions.
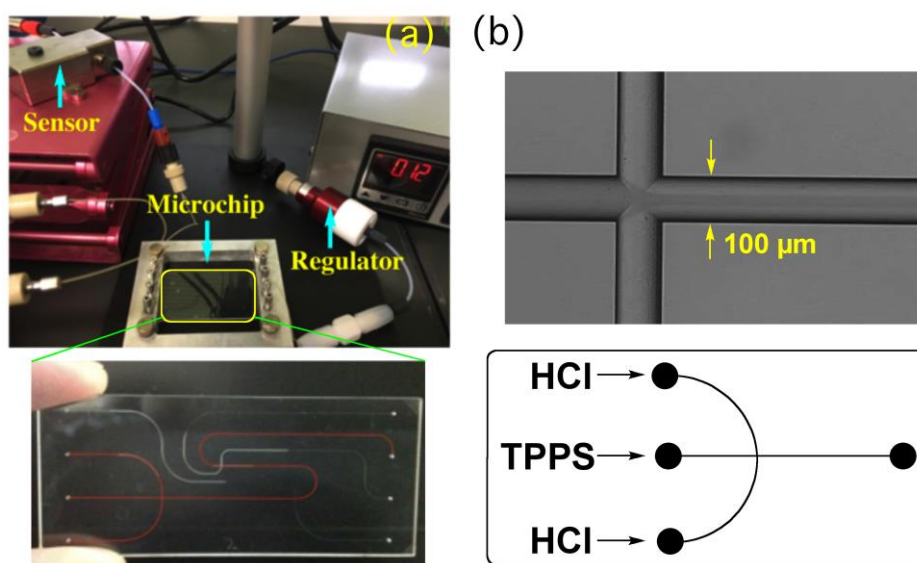

Figure 2. (**a**) Photograph of the microflow set-up (microflow chip equipped with a pressure regulator, pressure sensor, and pressure gauge) and enlarged image of microchip. (**b**) Photoimage of channel and schematic representation of the solution injection.

2. Materials and Methods

2.1. General

UV–Vis spectra were recorded using a JASCO V-670 apparatus. Microfluidic devices were purchased from the Institute of Microchemical Technology (IMT, Kanagawa, Japan) as custom-made products (see below). The pressure regulator was purchased from Device for Flow Chemistry (DFC, Kyoto, Japan) Pressure sensors were also obtained from DFC as custom-made products. TPPS was purchased from Tokyo Chemical Industry. All other reagents and solvents were purchased from Fujifilm Wako Pure Chemical Industries (Osaka, Japan), Tokyo Chemical Industry (Tokyo, Japan), Nacalai Tesque (Kyoto, Japan), and Aldrich (St. Louis, MO, USA).

2.2. Flow Design

Glass-made microchips were purchased from IMT as custom tips. The hydrodynamic flow was designed to focus three cross-points with a channel depth and width of 45 and 100 μm, respectively. The channel length from the inlet to the first cross-point was 18 mm. Aqueous HCl was injected from the first legs. The other legs in the lower stream were blocked with blind stoppers. The total channel length was 98 mm. The microchip was made of glass.

2.3. General Sample Preparation

Glass syringes containing 500 μL of the solution were placed on syringe pumps and connected to the aluminum jigs (microchip holder) by Teflon capillaries (length: 80 mm; inner diameter: 260 μm). The outlet of the microchip was connected to the Teflon capillaries and the solution was eluted into a glass vial under room temperature. After confirming a steady flow (generally, when at least 50 μL of the solution had eluted out), the solution was collected in a vial and subjected to spectroscopic measurement.

To regulate the pressure inside the channel precisely, a back-pressure regulator was connected at the outlet of the channel through a Teflon capillary.

The back-pressure applied inside the channel was measured using a pressure sensor, which was connected at the inlet and outlet of the channel through a Teflon capillary (Figure 2a). The pressure applied in the channel (ΔP) was calculated as the differential pressure, according to the following equation:

$$\Delta P = P_{\text{inlet}} - P_{\text{outlet}} \tag{1}$$

As a general example, an aqueous solution of TPPS (0.8 mM) was injected to the central stream at 10 μL min^{-1} under room temperature and squeezed by streams of aqueous HCl, the pH of which was either 3.0 or 5.0. The flow rate ratios (central flow/side flow) were fixed at 10/20, giving a total flow rate of 30 μL min^{-1}. The initial solution was, therefore, diluted to 0.267 mM (by 3 times) in the channel (Figure 2b). The final pH varied depending on the pH of the side HCl solutions; as measured, they were estimated to be 3.0 and 3.9, respectively.

3. Results and Discussion

Figure 3a presents a fluorescence microscopy image of a flowing solution of TPPS in a microflow channel. In this study, we injected aqueous hydrochloric acid as lateral solutions, resulting in protons always diffusing into the central thin-layered TPPS solution. In this particular system, the time required for proton diffusion was directly correlated to the width of the central flow, which we could control through the flow rate—a faster flow led to a narrower width (Figures 3b and 4a). Controlling the time for proton diffusion was essential because the effective self-assembly of TPPS molecules would occur only during periods of rapid proton diffusion. To evaluate the effect of the time on self-assembly quantitatively, the mole fraction of aggregated dye (α_{agg}) was defined as below:

$$\alpha_{\text{agg}} = \text{Abs}_{490}/(\text{Abs}_{434} + \text{Abs}_{490}) \times 100 \tag{2}$$

Figure 4c displays the α_{agg} with respect to the width of the central TPPS layer, as well as the time required for proton diffusion. The time required for proton diffusion in the channel was evaluated according to the reference (see the Supplementary Materials). We observe a direct correlation between the α_{agg} and the time required for proton diffusion.

Based on these results, next, we thoroughly examined how the rapid diffusion contributed to the total increase in the α_{agg} upon increasing the flow rate. To measure the back-pressure applied inside the channel, we connected a differential pressure gage to the inlet and outlet of the channel. According to the Hagen-Poisuille equation, the pressure applied inside the channel would be proportional to the flow rate (Figure 4b). Figure 4c summarizes the evaluated pressures at each flow rate (i.e., 10, 25, 50,

75, 100 µL/min). We observed a proportional correlation between the flow rate and back-pressure, in good accordance with the theoretical prediction.
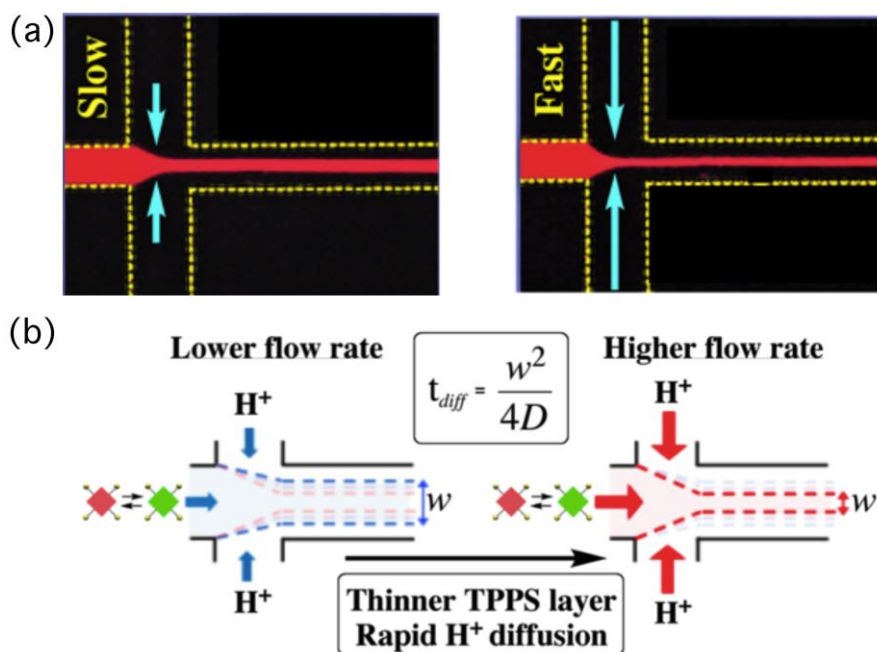

Figure 3. (**a**) Fluorescence microscopy images of an aqueous solution of TPPS injected from the central channel, and (**b**) a schematic representation of the effect of the flow rates on the width of the central flow (for the definition of t_{diff}; see the Supplementary Materials).

To subtract the effects of pressure on the self-assembly behavior of TPPS, we fixed the flow rate at 10 µL/min (width: 35.9 µm; diffusion time: 27.3 ms) and increased the pressure from 0.13 to 1.14 MPa by means of a back-pressure regulator connected at the end of outlet capillary (Figure 5a). Each pressure was regulated precisely to equal the back-pressure observed under each flow rate in Figure 4c. The width of the central layer (time required for proton diffusion) was always constant, regardless of pressure. Therefore, please note that this approach should reveal the effects of the pressure on the total α_{agg}. Figure 5b,c indicate that increasing the pressure caused the intensity of the absorption signal at 434 nm (corresponding to H_4TPPS) to decrease, whereas that at 490 nm (assignable to the J-aggregate) increased. Figure 5d summarizes the resultant α_{agg} obtained at each pressure. Plots of the α_{agg} with respect to pressure (Figure S1; red dots) revealed that the α_{agg} tended to increase slightly upon increasing the inner pressure (e.g., from 30.0 to 35.6% at pH 5). Considering the overall acceleration rates (i.e., from 30.0 to 54.2 % at pH 5), however, the observed increase rates were very minor. Therefore, we conclude that the pressure in the channel had little effect on the self-assembly, at least in the tested pressure range, suggesting that the accelerated self-assembly in the microflow was attributable mainly to the shorter diffusion time and simultaneous protonation. Given the limited effect of the back-pressure at pH 5, we performed the same experiments at pH 3. Fixing the flow rate at 10 µL/min (i.e., a diffusion time of 27.3 ms), we varied the back-pressure up to 1.1 MPa. Figure 5d summarizes the measured α_{agg}, in comparison with those obtained under pH 5. Figure 6a reveals that the pressure effect was more predominant than it was at pH 5, as expected because the concentration of H_4TPPS was increased at pH 3. We observed that the α_{agg} also tended to increase upon increasing the pressure, consistent with the behavior observed at pH 5. Nevertheless, it should be noted that the observed pressure effect remained very weak in terms of the total microflow effect.
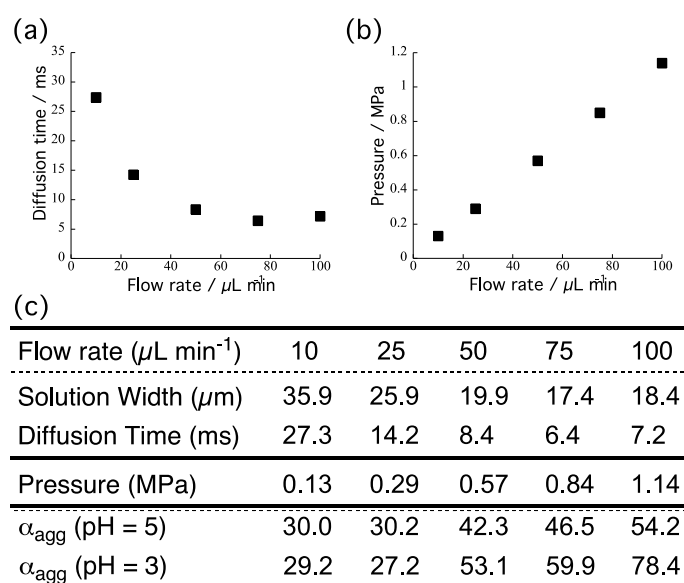
Figure 4. (**a**,**b**) Plots of (**a**) diffusion time of proton and (**b**) measured pressure against the flow rate in the channel. (**c**) Total aggregation efficiencies (α_{agg}) obtained upon changing the flow rate (for the plot, see Figure S1).

Flow rate (μL min^{-1})	10	25	50	75	100
Solution Width (μm)	35.9	25.9	19.9	17.4	18.4
Diffusion Time (ms)	27.3	14.2	8.4	6.4	7.2
Pressure (MPa)	0.13	0.29	0.57	0.84	1.14
α_{agg} (pH = 5)	30.0	30.2	42.3	46.5	54.2
α_{agg} (pH = 3)	29.2	27.2	53.1	59.9	78.4

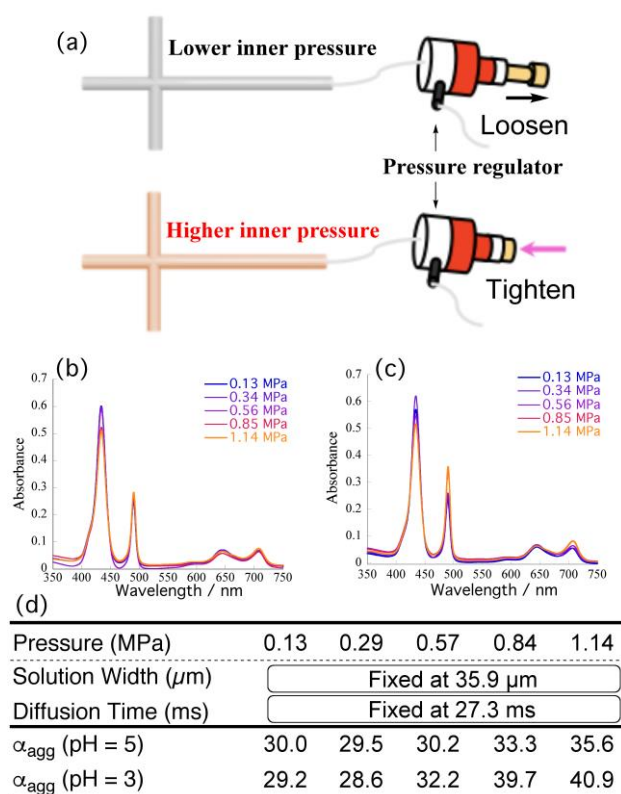| Pressure (MPa)	0.13	0.29	0.57	0.84	1.14
Solution Width (μm)		Fixed at 35.9 μm			
Diffusion Time (ms)		Fixed at 27.3 ms			
α_{agg} (pH = 5)	30.0	29.5	30.2	33.3	35.6
α_{agg} (pH = 3)	29.2	28.6	32.2	39.7	40.9

Figure 5. (**a**) Cartoon representation of the supramolecular polymerization of TPPS under the effect of back-pressure in the microflow channel. (**b**,**c**) UV–Vis spectra of TPPS recorded after increasing the back-pressure at pH (**b**) 5 and (**c**) 3 (under constant diffusion; i.e., v = 10 μL/min) (0.1 mm cell, r.t.). (**d**) Aggregation efficiencies measured upon varying pressure under a constant proton diffusion effect (for the comparison plot, see Figure S1).

To further certify the correlation between pressure effects and rapid proton diffusion, we performed the same experiments at higher flow rates of 25 and 50 µL/min (Figure S2). With much shorter diffusion times of 14.2 and 8.4 ms, respectively, we expected the pressure effect to be enhanced further because the temporal concentration of H_4TPPS would increase as a result of much faster proton diffusion. As expected, a flow rate of 25 µL/min caused the α_{agg} to increase more sensitively upon increasing the pressure than it did at 10 µL/min. This tendency was even clearer at 50 µL/min; that is, the slope in the plot (Figure 6b and Figure S3) became steeper at higher flow rates. Notably, a shorter diffusion time had the same effect as a lower pH on the self-assembly of TPPS. This finding strongly supports our view that very rapid proton diffusion led to an apparent decrease in pH in the area around H_2TPPS. In other words, protons could be concentrated on H_4TPPS through rapid protonation, resulting, ultimately, in a fixed state as a J-aggregate. Here, note again that the α_{agg} tended to increase upon increasing the inner pressure (e.g., from 29.7 to 35.2% under 25 µL/min at pH 5). With the overall acceleration rates (e.g., from 30.0 to 54.2% at pH 5) taken into consideration, however, the observed increase rates were still partial. The pressure effect on the α_{agg} became predominant only under the much faster proton diffusion conditions (i.e., at 50 µL/min). The pressure effect appeared depending on the concentration of H_4TPPS.
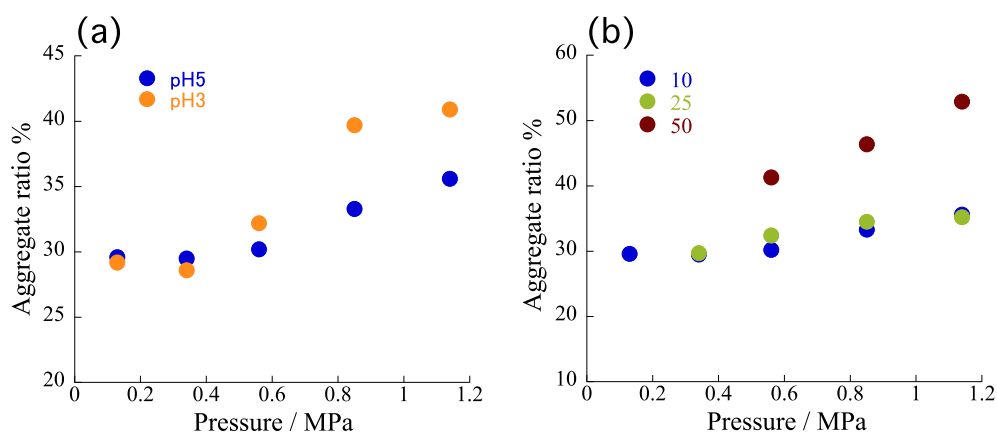

Figure 6. (**a**) Effects of proton concentration; comparative aggregation ratios at various values of pH, plotted with respect to pressure. (**b**) Pressure effects on the self-assembly efficiency at various proton diffusion times; plots of aggregation ratio with respect to pressure under various flow rates (pH 5). For the summarized values, see Figure S3.

This series of experiments has brought the pressure effect to the fore; it is an additional effect to consider, one that depends on the pH and/or the flow rates (i.e., the diffusion time of the protons). Lowering the pH and shortening the diffusion time (increasing the flow rates) would both lead to an increase in temporal H_4TPPS concentration. We conclude that the pressure effect was a secondary effect that appeared only under such a concentrated state of H_4TPPS.

Figure 7a summarizes the mechanism of the self-assembly process. TPPS obeys the cooperative polymerization mechanism, characterized by the existence of a nucleation process as a rate-determining step. Rapid diffusion of protons generated a temporally concentrated state of H_4TPPS. The activation energy for the nucleation step would decrease under such a concentrated state. Thus, shortening the diffusion time, which would cause the equilibrium shift toward H_4TPPS, would be essential for accelerating the self-assembly of TPPS (first step of Figure 7a). Increasing the pressure would accelerate the intermolecular interactions of H_4TPPS (second step of Figure 7a), which should occur especially at a higher H_4TPPS concentration, thereby leading to effective nucleation. As a feature point of self-assembly in microflow, same assembly processes occur in a parallel fashion along the channel. To clarify the self-assembly of a set of activated species along time progress, we propose a time-phase correlation scheme, among several equilibrium reactions, which would highlight the

synchronous behavior of molecules toward self-assembly (Figure 7b). Here, the synchronous behavior of molecules can be defined as the state that numerous numbers of molecules are under the same chemical environments in a restricted space and temporally behave as a sort of cluster, which would realize only through kinetic pathway under non-equilibrium. Synchronous behavior would allow more than thousands of molecules to acquire self-assembly abilities at the same timing, thus leading to acceleration of intermolecular interactions.
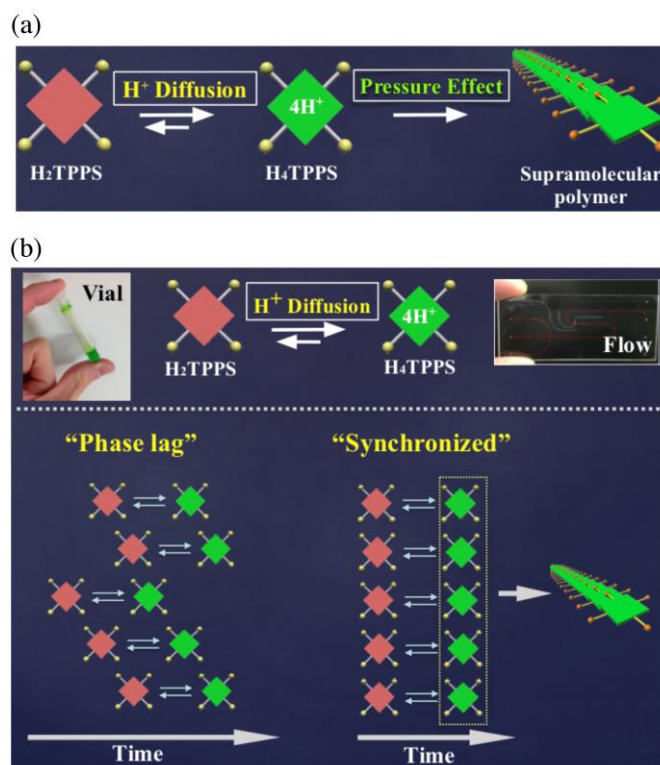

Figure 7. (**a**) Cartoon representation of the organized effects of proton diffusion and pressure on self-assembly. (**b**) Schematic representation of the synchronous behavior; cluster model of protonation/deprotonation equilibria along a time axis. Spontaneous protonation of H_2TPPS would lead to adjusting time phases of protonation/deprotonation reaction over the molecular scale (i.e., synchronizing toward self-assembly). This phenomenon would also induce long-range intermolecular interactions.

Finally, we have highlighted the effect of rapid proton diffusion on the self-assembly of TPPS. In this present system, laminar flow provided an environment for rapid and homogeneous proton diffusion. A micromixer would lead to further acceleration of proton diffusion into the TPPS solution, where a turbulent flow generated a fragmental solution on the micrometer scale. Following the laminar flow system, we injected the same TPPS solution from one leg into the channel of micromixer and mixed with aqueous hydrochloric acid injected from another leg. Notably, as summarized in Figure S4, the pressure measured inside the channel was almost equal to atmospheric pressure, even at higher flow rates; therefore, pressure effects would be negligible in comparison with that in a flow focus-type microchannel. Nevertheless, the α_{agg} remained high on average, even at lower flow rates. Accordingly, we attribute the observed accelerated effects on the protonation and self-assembly of TPPS to the very rapid diffusion of protons [19].

4. Conclusions

In summary, we have elucidated how the microflow environment affects molecular self-assembly by employing the supramolecular polymerization of TPPS as a model. Back-pressure has, in essence, a negligible effect on the self-assembly; it appeared only when H_4TPPS was temporally concentrated through rapid protonation (i.e., for shorter diffusion times). We propose, therefore, that there is a strong correlation between the time required for protonation of H_2TPPS and its ability to self-assemble. Simultaneous protonation of all H_2TPPS species enforced synchronization of the time phase of their protonation/deprotonation equilibria, thereby leading to a temporal increase in the H_4TPPS concentration. Looking at the results in another way, even a very weak pressure could be a trigger for self-assembly when coupled with synchronous molecular behavior. We hope that these findings will open new doors for molecular self-assembly.

Supplementary Materials: The following are available online at http://www.mdpi.com/2073-4352/8/7/300/s1, Figure S1: Total aggregation efficiency upon changing the flow rate (including both pressure and diffusion effects; blue dots) and extracted pressure effects under constant proton diffusion effect at 10 μL/min (red dots); (a) pH 5; (b) pH 3; Figure S2: UV–Vis spectral changes of TPPS upon changing the pressure inside the channel at pH 5; v = (a) 10, (b) 25, and (c) 50 μL/min. 0.1 mm cell, r.t; Figure S3: Effects of proton diffusion time on aggregation efficiency upon changing the back-pressure inside the channel; summary of extracted pressure effects on aggregation efficiency; Figure S4: Effects of proton diffusion time on aggregation efficiency in turbulent flow.

Author Contributions: M.N. conceived and designed the experiments; C.K. performed the experiments and analyzed the data; M.N. wrote the paper.

Conflicts of Interest: The authors declare no conflict of interest.

References

1. Numata, M.; Sakai, R. Kinetically controllable supramolecular polymerization through synchronized activation of monomers. *Bull. Chem. Soc. Jpn.* **2014**, *87*, 858. [CrossRef]
2. Numata, M.; Sakai, R.; Asai, A.; Sanada, Y.; Sakurai, K. Controlled nucleation of supramolecular polymerization in a pressure-regulatable microflow channel. *Chem. Lett.* **2015**, *44*, 1601. [CrossRef]
3. Collings, P.J.; Gibbs, E.J.; Starr, T.E.; Vafek, O.; Yee, C.; Pomerance, L.A.; Pasternack, R.F. Resonance light scattering and its application in determining the size, shape, and aggregation number for supramolecular assemblies of chromophores. *J. Phys. Chem. B* **1999**, *103*, 8474. [CrossRef]
4. Pasternack, R.F.; Fleming, C.; Herring, S.; Collings, P.J.; de Paula, J.; DeCastro, G.; Gibbs, E.J. Aggregation kinetics of extended porphyrin and cyanine dye assemblies. *Biophys. J.* **2000**, *79*, 550–560. [CrossRef]
5. Kano, K.; Fukuda, K.; Wakami, H.; Nishiyabu, R.; Pasternack, R.F. Factors Influencing Self-Aggregation Tendencies of Cationic Porphyrins in Aqueous Solution. *J. Am. Chem. Soc.* **2000**, *122*, 7494–7502. [CrossRef]
6. Schwab, A.D.; Smith, D.E.; Rich, C.S.; Young, E.R.; Smith, W.F.; de Paula, J. Porphyrin Nanorods. *J. Phys. Chem. B* **2003**, *107*, 11339–11345. [CrossRef]
7. Okada, S.; Segawa, H. Article Previous Article Next Article Table of Contents Substituent-Control Exciton in J-Aggregates of Protonated Water-Insoluble Porphyrins. *J. Am. Chem. Soc.* **2003**, *125*, 2792–2796. [CrossRef] [PubMed]
8. Rotomskis, R.; Augulis, R.; Snitka, V. Hierarchical Structure of TPPS$_4$ J-Aggregates on Substrate Revealed by Atomic Force Microscopy. *J. Phys. Chem. B* **2004**, *108*, 2833–2838. [CrossRef]
9. Jahn, A.; Vreeland, W.N.; Gaitan, M.; Locascio, L.E. Controlled vesicle self-assembly in microfluidic channels with hydrodynamic focusing. *J. Am. Chem. Soc.* **2004**, *126*, 2674–2675. [CrossRef] [PubMed]
10. Shinohara, K.; Sugii, Y.; Hibara, A.; Tokeshi, M.; Kitamori, T.; Okamoto, K. Rapid proton diffusion in microfluidic devices by means of micro-LIF technique. *Exp. Fluids* **2005**, *38*, 117–122. [CrossRef]
11. Pfohl, T.; Otten, A.; Köster, S.; Dootz, R.; Struth, B.; Evans, H.M. Highly packed and oriented DNA mesophases identified using in situ microfluidic X-ray microdiffraction. *Biomacromolecules* **2007**, *8*, 2167–2172. [CrossRef] [PubMed]

12. Karnik, R.; Gu, F.; Basto, P.; Cannizzaro, C.; Dean, L.; Kyei-Manu, W.; Langer, R.; Forokhzad, O.C. Microfluidic platform for controlled synthesis of polymeric nanoparticles. *Nano Lett.* **2008**, *8*, 2906–2912. [CrossRef] [PubMed]

13. Puigmartí-Luis, J.; Schaffhauser, D.; Burg, B.R.; Dittrich, P.S. A microfluidic approach for the formation of conductive nanowires and hollow hybrid structures. *Adv. Mater.* **2010**, *22*, 2255–2259. [CrossRef] [PubMed]

14. Suga, S.; Yamada, D.; Yoshida, J.-I. Cationic three-component coupling involving an optically active enamine derivative. From time integration to space integration of reactions. *Chem. Lett.* **2010**, *39*, 404–406. [CrossRef]

15. Numata, M. Supramolecular Chemistry in Microflow Fields: Toward a New Material World of Precise Kinetic Control. *Chem. Asian J.* **2015**, *10*, 2574–2588. [CrossRef] [PubMed]

16. Numata, M.; Sato, A.; Nogami, R. Energy-dissipative Self-assembly Driven in Microflow: A Time-programmed Self-organization and Decomposition of Metastable Nanofibers. *Chem. Lett.* **2015**, *44*, 995–997. [CrossRef]

17. Pumera, M. Nanomaterials meet microfluidics. *Chem. Commun.* **2011**, *47*, 5671–5680. [CrossRef] [PubMed]

18. Puigmartí-Luis, J. Microfluidic platforms: A mainstream technology for the preparation of crystals. *Chem. Soc. Rev.* **2014**, *43*, 2253–2271. [CrossRef] [PubMed]

19. Sorrenti, A.; Rodriguez-Trujillo, R.; Amabilino, D.B.; Puigmartí-Luis, J. Milliseconds Make the Difference in the Far-from-Equilibrium Self-Assembly of Supramolecular Chiral Nanostructures. *J. Am. Chem. Soc.* **2016**, *138*, 6920–6923. [CrossRef] [PubMed]